Journal of the European Ceramic Society 36 (2016) 1571–1580

Contents lists available at www.sciencedirect.com

Journal of the European Ceramic Society

journal homepage: www.elsevier.com/locate/jeurceramsoc

Development of wound $SiC_{BNx/SiNx}$/SiC with near stoichiometric SiC matrix via LSI process

Bernd Mainzer[a,*], Kristina Roder[b], Lydia Wöckel[c], Martin Frieß[a], Dietmar Koch[a], Daisy Nestler[b], Daniel Wett[b], Harry Podlesak[b], Guntram Wagner[b], Thomas Ebert[c], Stefan Spange[c]

[a] Institute of Structures and Design, German Aerospace Center (DLR), Pfaffenwaldring 38-40, 70569 Stuttgart, Germany
[b] Chair of Composite Materials, Technische Universität Chemnitz, 09107 Chemnitz, Germany
[c] Chair of Polymer Chemistry, Technische Universität Chemnitz, 09107 Chemnitz, Germany

ARTICLE INFO

Article history:
Received 24 September 2015
Received in revised form
11 December 2015
Accepted 14 December 2015
Available online 22 January 2016

Keywords:
Ceramic matrix composites
SiC/SiC
LPCVD
Phenolic resin
β-Naphthol

ABSTRACT

In order to develop SiC/SiC ceramic matrix composites with a low porosity, liquid silicon infiltration (LSI) was chosen as a technique, characterized by short processing times. To create the matrix, a tailored phenolic resin containing ß-naphthol units was synthesized and infiltrated in wound fiber preforms, thermally cured, pyrolysed and siliconized. The aim is to obtain a high carbon yield during pyrolysis and to create a dense carbon foam between the SiC fibers. Instead of a classic liquid silicon infiltration via capillary forces through a carbon block-like microstructure, this foam promotes a softer infiltration with less fiber degradation and a maximized carbon conversion to near stoichiometric SiC. To protect the SiC fibers from an attack of the liquid silicon and to simultaneously provide a weak fiber matrix bonding, a BN_x/SiN_x fiber coating was chosen. The coating was applied by means of low-pressure chemical vapor deposition (LPCVD) using gaseous chlorine free precursors.

1. Introduction

To obtain SiC/SiC composites, liquid silicon infiltration process [1,2] has been chosen. It is a three-stage process, beginning with the infiltration of a SiC fiber-preform with a resin (Fig. 1, step I). Resin transfer molding (RTM) was used as a production technique, allowing a homogeneous infiltration of resins and controlling temperature and pressure during the curing process, which results in a dense SiC fiber-reinforced polymer (SiCFRP). An additional pyrolysis step transforms the polymer matrix to carbon with a porous structure, creating a SiC fiber-reinforced carbon (SiC/C) (Fig. 1, step II). The final step of the process is the infiltration of liquid silicon into the pores. This is achieved by capillary forces and results in the conversion of the carbon matrix to a SiC matrix in an exothermic reaction (SiC/SiC).

Previous research has shown that a single coating layer of SiN_x on SiC fibers is resistant against liquid silicon but did not provide damage tolerant crack behavior. The phenolic resin utilized was also unsuitable, as it shrinks to form dense carbon blocks during pyrolysis and long hollow channels along the fibers [3–5]. These channels were filled with large amounts of silicon, which was found to be fairly aggressive to the coating. The carbon blocks were not infiltrated with liquid silicon to form SiC. Thus, C and Si remain in the composite which might be disadvantageous at application conditions. In order to improve the carbon conversion and to decrease the amount of free silicon, a novel resin was developed (Fig. 1, step 0″) that has shown to create a carbon-foam in composites with uncoated SiC fibers during processing, rather than carbon blocks. Furthermore, to create composites with damage tolerant crack behavior, a novel double coating technique was utilized. The inner layer consisted of BN_x and the outer layer is comprised of SiN_x (Fig. 1, step 0′). The SiN_x layer serves as a protective coating against liquid silicon [6], while the inner BN_x layer creates a weak interface, which is needed in SiC/SiC composites to provide energy dissipating effects like crack deflection, crack bridging and fiber pull-out to create a pseudo-ductile and therefore damage tolerant composite [7].

* Corresponding author.
E-mail address: bernd.mainzer@dlr.de (B. Mainzer).

http://dx.doi.org/10.1016/j.jeurceramsoc.2015.12.015

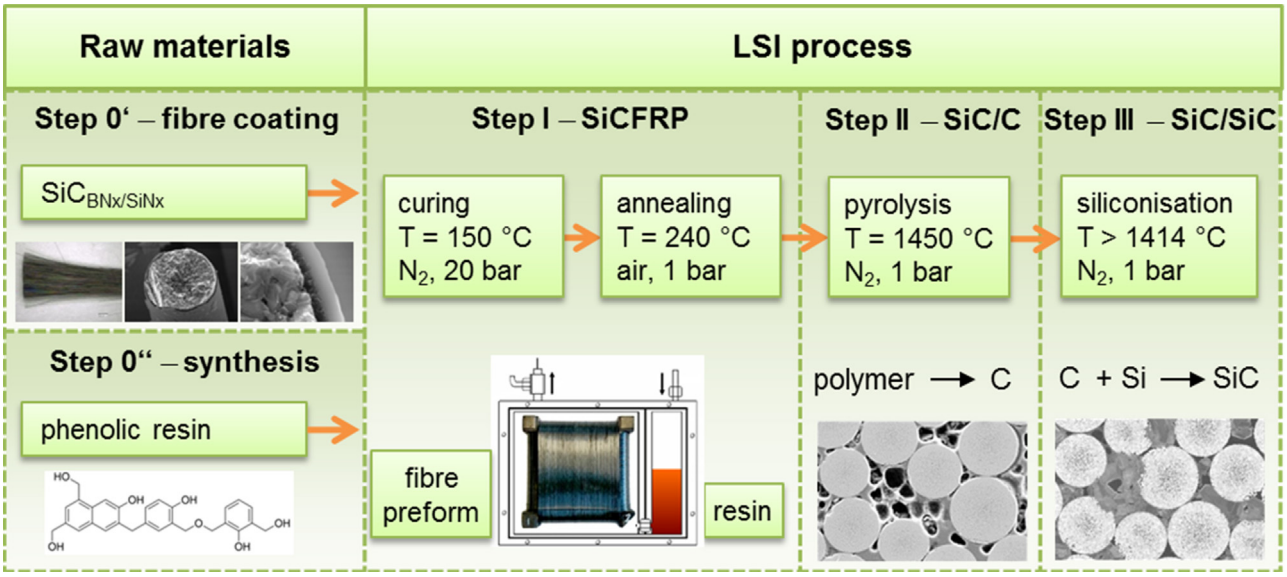

Fig. 1. Scheme of the LSI process.

2. Experimental procedure

2.1. Development of BN_x/SiN_x fiber coating (Step 0′)

The commercial SiC fiber Tyranno SA3 from UBE Industries was used for coating experiments. The yarn consists of 1600 single filaments with a diameter of 7.5 μm [8]. The coating was applied by means of low-pressure chemical vapor deposition (LPCVD). The process was carried out discontinuously in a horizontal tubular hot-wall reactor of the laboratory system TCVD 100 LAB from FHR Anlagenbau. For the coating process the CVD system was evacuated. The reactor was heated until the processing temperature was achieved. Simultaneously, the gas supply system and the reactor were purged with nitrogen. During this step, the fibers were desized in-situ. The BN_x coating took place at a temperature of 975 °C. The gaseous precursors diborane (B_2H_6) diluted in 95 vol% hydrogen (H_2) and ammonia (NH_3) were introduced to the reactor with a constant flow rate of 100 and 150 sccm. The mixing ratio of NH_3/B_2H_6 was 30:1. The pressure was set to 3 mbar using a butterfly valve. The coating time was 60 min. For the SiN_x coating a temperature of 800 °C was used. Furthermore, the flow rate for the deposition was set to 12.5 sccm silane (SiH_4) and 125 sccm ammonia (NH_3) and a pressure of 1 mbar was also adjusted. All in all the SiN_x coating took 30 min. After the coating process the gas supply system and the reactor were purged with nitrogen again and the reactor cooled down.

The coated fibers were subjected to a high-temperature heat treatment in order to examine the stability of the films under the processing conditions of the LSI process. The fibers were treated in a furnace (Ing.Büro Vakuumtechnik, Anl.Nr. 9055) at a temperature of 1450 °C in nitrogen for 30 min.

2.2. Synthesis of the R2 phenolic resin (Step 0″)

The phenol-β-naphthol-formaldehyde resol R2 was synthesized according to the procedure as described in the literature [3]. For the synthesis, 100.0 g (1.06 mol) phenol, 76.6 g (0.53 mol) β-naphthol, 237 ml formalin (37 wt%; 3.18 mol) and a 3 M aqueous sodium hydroxide solution (8.9 g; 0.22 mol) as catalyst were used. The obtained phenol-β-naphthol-formaldehyde resol R2 (263.2 g) is a red liquid at room temperature (RT). It reaches its minimum viscosity of 0.31 Pa·s at 102 °C and the self-curing begins at approximately 110 °C, which was determined with differential scanning calorimetry and rheology measurement [3]. For a better understanding of the mechanisms during the different steps of the LSI process within the fiber-reinforced composites, pure specimens of the R2 resin were investigated under the processing conditions.

2.3. CMC manufacturing with coated fibers and R2 phenolic resin (Step I–III)

A flat graphite mandrel was manufactured to provide a fiber preform. A total of eight cross-ply layers with an orientation of 0/90° of uncoated Tyranno SA3 fibers were wound on the mandrel (Fig. 2). Between the fourth and fifth layers a BN_x/SiN_x-coated SA3 roving was manually integrated. After being wound, the mandrel was infiltrated with the R2 resin at the temperature of minimum viscosity by means of resin transfer molding. After being fully infiltrated, the curing process was realized at a temperature of 150 °C and a pressure of 20 bar in a nitrogen atmosphere. The infiltrated preform was cut, leading to two long fiber-reinforced plates with the size of $60 \times 60 \times 2\ mm^3$ and a fiber volume content of 47%. Afterwards, the plates were annealed in an ambient atmosphere at 240 °C, resulting in the creation of a silicon carbide fiber reinforced polymer (SiCFRP).

The SiCFRP was pyrolysed at 1450 °C in a nitrogen atmosphere and a pressure of 1 bar to convert the polymer matrix to a carbon matrix. This was followed by a silicon infiltration at a temperature just above the melting point of silicon at 1415 °C and the same pressure and atmospheric conditions. The silicon was infiltrated in the plates from above by means of gravity. The same furnace (Ing.Büro Vakuumtechnik, Anl.Nr. 9055) was used for the pyrolysis and for the infiltration.

2.4. Characterization methods

2.4.1. NMR

The carbon nuclear magnetic resonance spectroscopy measurement (liquid ^{13}C NMR) was performed with a Bruker Avance 250 MHz spectrometer. Deuterated acetone-d_6 (C_3D_6O) was used as a solvent for the uncured R2. The samples were referred to the solvent (C_3D_6O $\delta = 2.05$ ppm).

For the solid state carbon cross polarization magic angle spinning measurement (^{13}C CPMAS) of cured R2 a Bruker

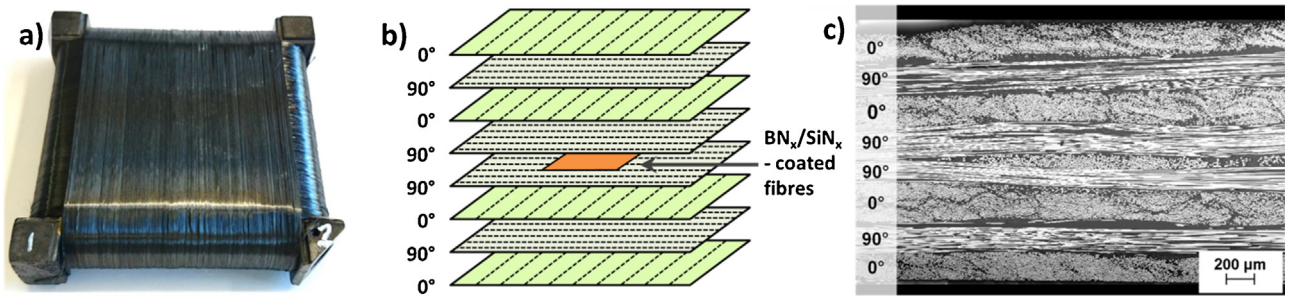

Fig. 2. Fiber preform: (a) SiC fibers wound on graphite mandrel; (b) scheme of the wound layers: 8 layers 0/90 cross-ply with BN_x/SiN_x-coated fibers in the center; (c) SEM cross section of SiCFRP.

Avance 400 MHz was used. The extern standard was adamantane (δ = 38.48 ppm) and the rotation frequency 15 kHz.

2.4.2. Elemental analysis

The elemental analysis was carried out with a Vario El from the company Elementaranalysensysteme GmbH.

2.4.3. Microstructural analysis

The microstructure of the fibers was analyzed on polished sections and fracture surfaces by means of scanning electron microscopy (SEM, LEO 1455VP and NEON 40EsB, Zeiss). Additionally, transmission electron microscopy studies (TEM, HITACHI H8100) were performed on mechanically and argon ion-milled thin sections with an acceleration voltage of 200 keV. For the selected area electron diffraction (SAED) the smallest area aperture had a diameter of 600 nm.

The microstructure of the polymer, carbon and composite samples were investigated on polished sections by optical microscopy (GX51, Olympus Stream, Olympus) and scanning electron microscopy (Gemini Ultra Plus, Zeiss).

2.4.4. X-ray diffraction

The X-ray diffraction (XRD) measurements on the fiber yarns were carried out utilizing the D8 DISCOVER from Bruker with an area detector. The Co Kα radiation was used.

2.4.5. Raman spectroscopy

The Raman spectroscopic measurements were performed with a confocal Raman microscope (50× Leica objektive) inVia Reflex from Renishaw, which is equipped with a deep depletion CCD array detector (1024 × 256 Pixel). For the fibers a HeNe laser with a wavelength of 633 nm was used, while the carbon samples and SiC/C composites were analyzed by a frequency-doubled Nd:YAG laser with a 532 nm wavelength.

2.4.6. Water infiltration

The open porosity of polymers and composites were determined via the Archimedes water infiltration method (DIN EN 993-1).

2.4.7. He-pycnometry

The densities were calculated from the mass and the volume of the carbon materials of R2. With a Multi Pycnometer from Quantachrome and helium gas, the volumes of the bulk and pulverized carbon were determined.

2.4.8. Hg-porosimetry

In order to obtain the density and open porosity, intrusion and extrusion curves were measured. With a Pascal 140 mercury porosimeter (Thermo Scientific) the pores were studied at a low pressure. The analysis of the pores was carried out at a high pressure, utilising a Porosimeter 2000 (Fisons Instruments).

2.4.9. Contact angles

The contact angles of molten silicon on different surfaces were measured with a DSAHT17-1 from Krüss GmbH in an argon atmosphere.

3. Results and discussion

3.1. Characterisation of the coated fibers (Step 0′)

The cross sectional images of the coated fibers of the center of the yarn and of the edges (Fig. 3a and b) shows the uniform thickness of the dark grayed BN_x-coating. The SiN_x-coating on the other hand displays a gradient of the thickness from the center to the edges [4]. Furthermore, the thickness of the coating on the edge is inhomogeneous, resulting in an ellipse-like shape. The double coating (Fig. 3c) is characterized by an excellent connection to the SiC fiber. There are no delaminations or pores at the coating/fiber interface.

The high-temperature heat treatment results in partially cracking of the double coating. The crack formation can be explained by the residual stresses within the coating, which are a sum of any thermal and intrinsic stresses. Especially the thicker coating at the edge of the yarn tends to crack. The thinner coating of the center of the yarn is crack free. The BN_x-coating does not show any changes after undergoing the heat treatment (Fig. 4). In contrast, pores and precipitations are formed within the SiN_x-coating on fibers in the center of the yarn and on the edges, respectively.

Fig. 5 shows the results of the XRD measurements on the fiber yarns. Reflections for the cubic SiC phase are dominant for the uncoated fibers. The (1 1 1) reflection of the cubic SiC at 41.7° displays an additional shoulder at smaller angles, which correlates with the hexagonal SiC phase [9]. The cubic and hexagonal modifications of SiC differ in their stacking sequences of atomic planes and both can occur in the same grain. Stacking faults confine the neighboring regions with different SiC crystal modifications. The resulting lamellar structure of SiC grains can be seen at the fracture surfaces in Fig. 4. A very fine lamination can reduce or prevent the detectability of the SiC phases. Due to these reasons the XRD results show no clear results.

The double-coated fibers show no additional reflections. It can be concluded that both coatings are amorphous. The heat treatment results in a crystallisation of the SiN_x-coating. The corresponding diffractogram reveals the reflections of a trigonal α-Si_3N_4 phase. In addition, traces of cubic Si are present. A crystalline BN phase is not detectable.

The Raman spectra of single fibers from the center of the yarn and the edge of the yarn confirm the results of the XRD measurements (Fig. 6). The spectrum of an uncoated fiber exhibits characteristic peaks for the cubic SiC phase (796 and 972 cm^{-1}). The shoulder at 764 cm^{-1} can be explained by the hexagonal SiC phase [10]. The free carbon within the SiC fiber generates the typical peaks

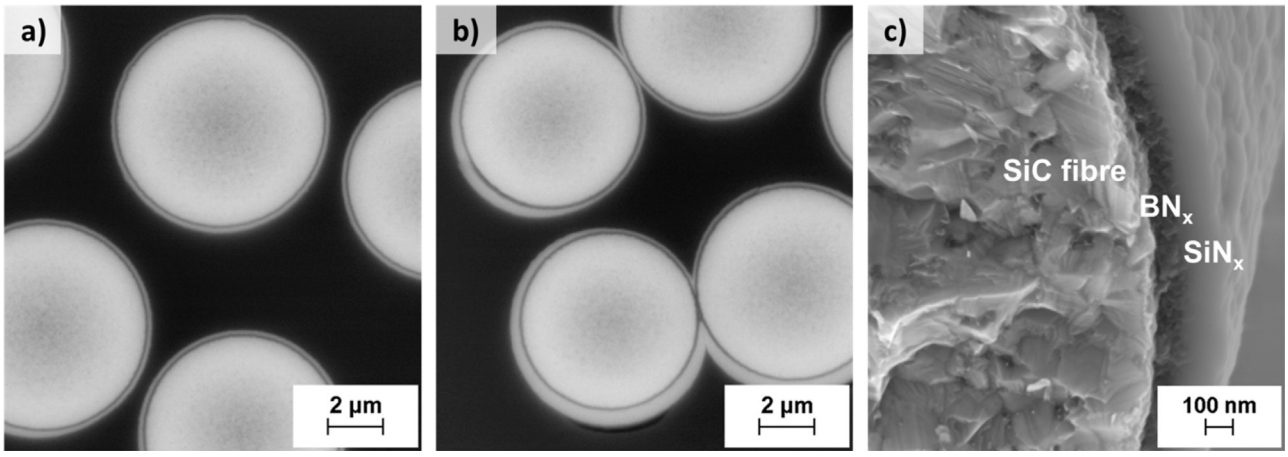

Fig. 3. BN_x/SiN_x-coated fibers: (a) polished section of the center of the yarn (SEM); (b) polished section of the yarn edge (SEM); (c) fracture surface (SEM).

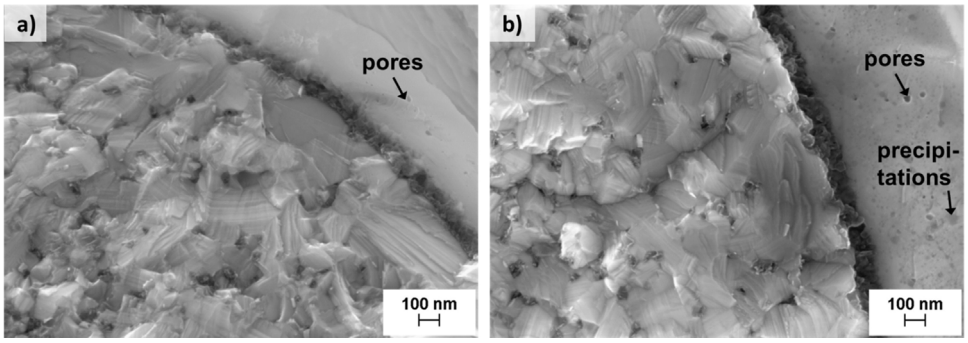

Fig. 4. Heat-treated BN_x/SiN_x-coated fibers: (a) fracture surface of a fiber of the center of the yarn (SEM); (b) fracture surface of a fiber of the yarn edge (SEM).

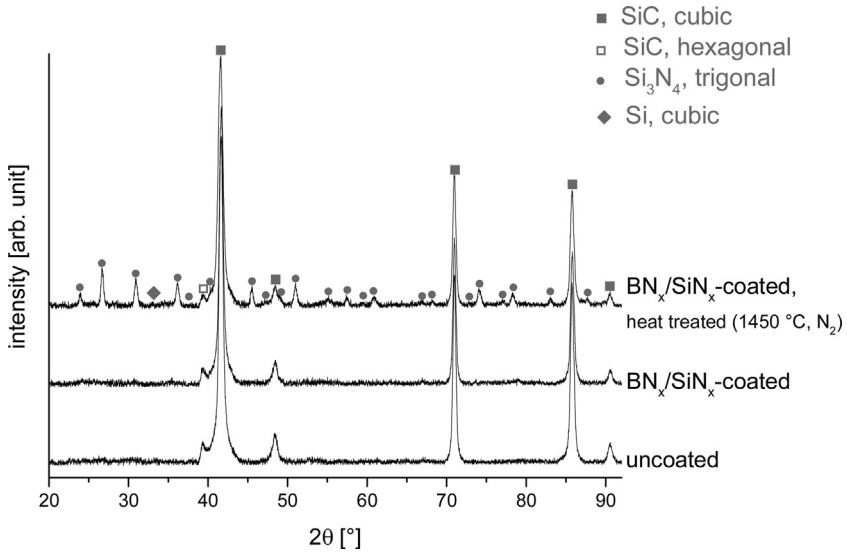

Fig. 5. X-ray diffractograms of the uncoated and BN_x/SiN_x-coated fiber yarns, as well as the ones, which underwent heat-treatment.

the D band and the G band [9]. The spectra of the coated fibers from the center of the yarn and the edge of the yarn have no additional peaks of the BN and Si_3N_4 phase, which can be attributed to the amorphous character of the coatings. It has to be mentioned, that the expected BN peak overlaps with the D band of the carbon. For this reason, it is difficult to detect BN. After the heat treatment only the characteristic peaks of the Si_3N_4 phase are present. In addition, the spectrum of a thicker coating at the edge of the yarn displays an additional peak for Si, which is a result of the precipitations (Fig. 4b).

Fig. 7 displays the TEM image of a coated fiber after the deposition process. The BN_x coating shows some disordered features typical for amorphous structures, whereas the SiN_x coating has no visible details. The information of the diffraction pattern is limited, due to the fact of the thickness of the layers being smaller than the diameter of the aperture. Two broadened rings indicate either one or both coatings being amorphous. The diffraction spots are generated from the SiC grains of the fiber.

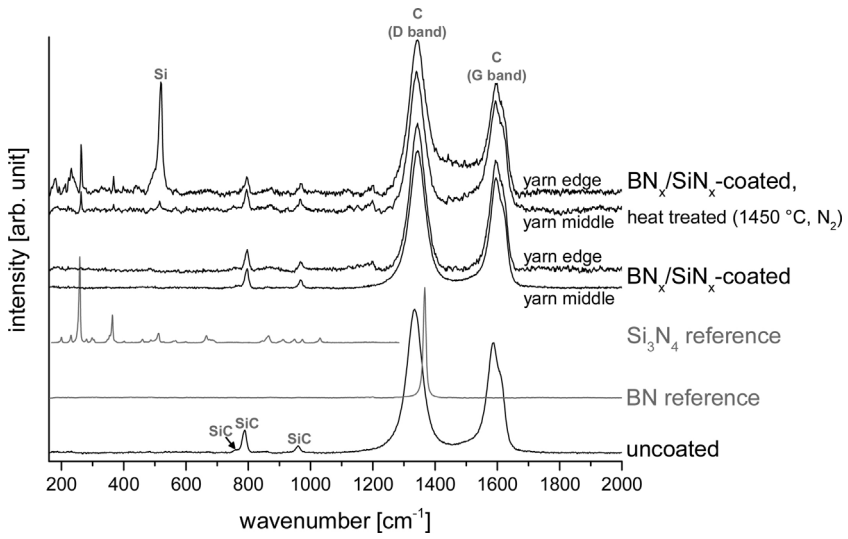

Fig. 6. Raman spectra of the uncoated, BN_x/SiN_x-coated and of the heat-treated BN_x/SiN_x-coated fibers in comparison with reference spectra of Si_3N_4 and BN.

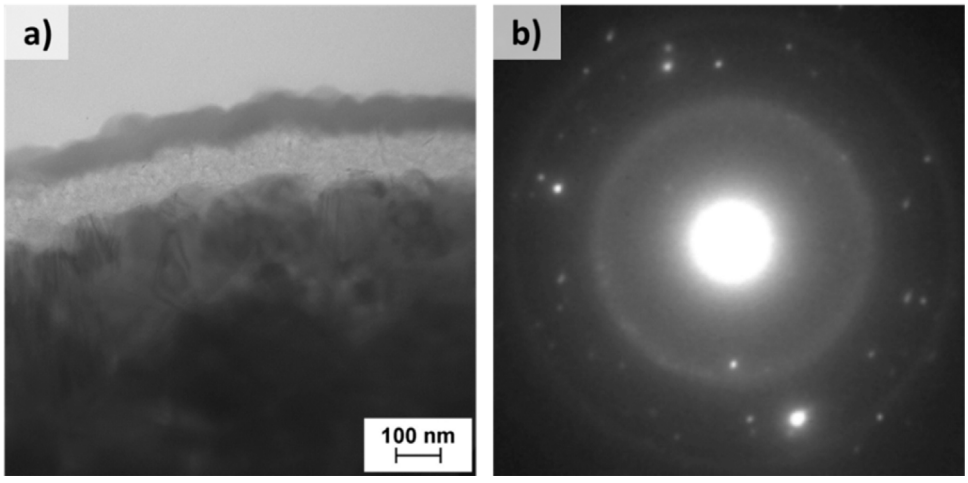

Fig. 7. BN_x/SiN_x-coated fibers: (a) bright field TEM image; (b) selected area diffraction pattern.

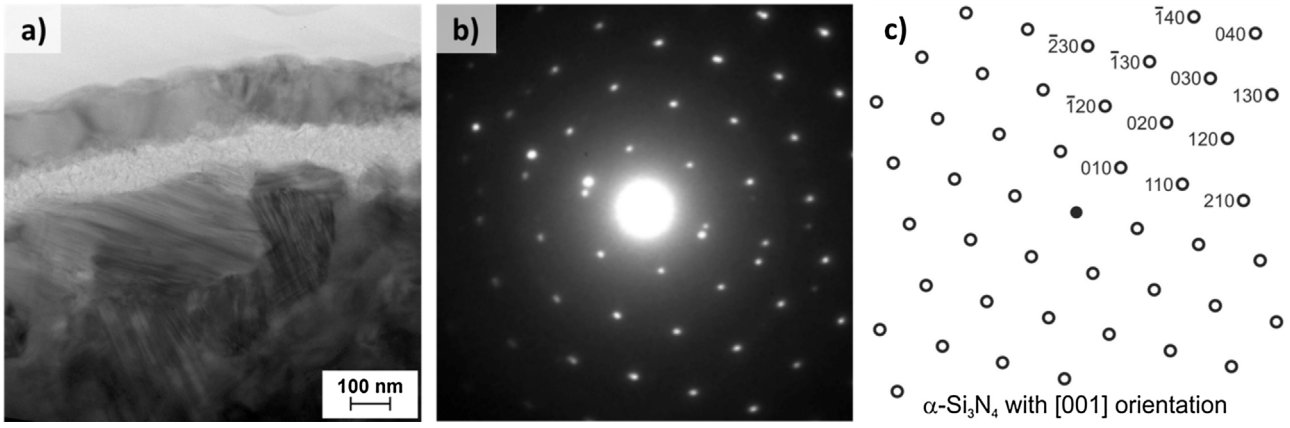

Fig. 8. Heat-treated BN_x/SiN_x-coated fibers: (a) bright field TEM image; (b) selected area diffraction pattern; (c) indexing of the mono crystal diffraction pattern.

Subsequent to undergoing the heat treatment the double coating looks similar to the untreated fibers (Fig. 8), but the diffraction pattern indicates the crystallization. The pattern includes spots of two grains, which can be attributed to a trigonal α-Si_3N_4 phase with a submicron grain size. The BN_x coating does not contribute to the diffraction pattern.

In conclusion, the deposition process by means of LPCVD results is an amorphous double coating, for which the thickness of the BN_x coating is very uniform. The SiN_x coating shows a gradient

of the coating-thickness from the center of the yarn to the edges. The deposition is controlled by the transport mechanism of the gaseous reactants inside the fiber yarn, leading to a depletion of the reactants. In addition there is also a gradient of the chemical composition within the SiN_x coating. The coating is rich in Si at the edges of the yarn, which leads to Si precipitations during heat treatment. In the center of the yarn a higher amount of hydrogen or nitrogen is present, resulting in the formation of pores during the heat treatment. The diffusion of the reactants occurs in Knudsen regime [11]. The diffusion coefficient of NH_3 is higher than the one of SiH_4, which leads to a depletion of SiH_4 in the center of the yarn. This results in the formation of a gradient of the chemical composition [4]. During the heat treatment only the SiN_x coating crystallizes to a trigonal α-Si_3N_4.

Over the course of the thermal treatment the thicker coating at the edge of the yarn is prone to crack. The majority of the coating on fibers in the center of the yarn remains stable. As a result of these findings, the double coating was chosen for the LSI process.

3.2. Characterisation of the R2 phenolic resin and the polymer matrix (Step 0″ and Step I)

The obtained β-naphthol containing resol R2 consists of low condensed oligomers and its solubility in acetone allows an analysis by means of liquid-^{13}C NMR spectroscopy (Fig. 9). It shows signals for methylene (A) (29–42 ppm), methylol (B) (58–63 ppm) and methylenether (C) (65–75 ppm) groups. The signal at 88 ppm can be assigned to hemiformal structures (D) where aryl hydroxy groups condensate with hydrated formaldehyde ($HO—CH_2—OH$) or formaldehyde dimers [12–14].

During a thermal curing at 150 °C the methylol and methylenether groups react to methylen bridges under a condensation of water. With solid state carbon NMR (^{13}C CPMAS-NMR) the insoluble, cured polymer (P) can be characterized. The ^{13}C CPMAS-NMR spectra (Fig. 9) of the R2 cured at 150 °C shows broad signals with low intensities which can be caused by incomplete condensed methylol (B) and methylenether (C) groups. Furthermore, the additional exothermic peak at 175 °C in the DSC curves [3] indicates a subsequent condensation of the polymer. This shows the necessity of an annealing of the polymer for the post-condensation at elevated temperatures. The small signal at 171 ppm can be attributed to benzoic acid carbon (—COOH), which can be formed by dehydrogenation and oxidation [15]. In both, liquid and solid state ^{13}C NMR spectra, the aryl carbon (C_{Aryl}-OH) attached to the hydroxy group can be found between 148 and 160 ppm and non-hydroxy aryl carbon (C_{Aryl}) can be found between 111 and 137 ppm [12–16].

The polymer obtained after curing at 150 °C and an increased pressure of 20 bar was analysed by means of optical microscopy and SEM. The pure cured polymer (P) (Fig. 10a) and the SiCFRP (Fig. 10b) prior to undergoing the pyrolysis process show pores in the range of 1–3.2 μm distributed over the whole sample. This indicates the development of the pores during the curing process. One possible explanation might be the formation of water over the course of the condensation reaction of the methylol and methylenether groups. However, β-naphthol as a component in resol, is important for the formation of pores, because the resol formulation without the β-naphthol shows no pores during same curing conditions [3]. Additionally, the pore-formation creates foam between the SiC fibers. This can be seen in the SEM image (Fig. 10b) of SiCFRP, which shows no sign of matrix/fiber debonding. In case of the $SiC_{BNx/SiNx}$FRP sample a lot of matrix/coating debondings are present (Fig. 10c). The adhesive forces at the interface are insufficient. As a result of the debonding an unhindered volume-shrinkage of the polymer matrix occurs, which leads to the formation of dense polymer blocks with hollow channels along the coated fibers. This means the formation of pores within the polymer matrix is locally supressed. Some debondings are also present at the fiber/coating interface. The coating was partly cracked and detached along the inner BN_x interface.

3.3. Characterisation of the pure carbon and the carbon matrix (Step II)

After undergoing the curing and annealing process, as well as the pyrolysis the pure R2 suffers from an overall loss of 48.8 wt% of its mass. The quantitative elemental analysis of the carbon revealed a hydrogen and carbon content of 0.23% and 98.41%, respectively.

Margiotta et al. show that the carbon needs to have pores with a diameter over 1 μm to prevent a pore choking during silicon infiltration caused by the formation of SiC [17]. The carbon (C) and the SiC/C matrix, which were obtained from the R2 show pores between 1–4.5 μm (Fig. 11a and b). In addition, after undergoing pyrolysis there is no delamination of the matrix from the SiC fibers to be observed, indicating a strong fiber/matrix bonding. In case of the BN_x/SiN_x-coated fibers the matrix shrank further, leading to the degradation of the coating (Fig. 11c). Additionally, the boron nitride layer can be decomposed by NaOH [18], which was present in the R2 resin. Due to the synthesis, a content of 3.4 wt.-% of NaOH remains in R2. Lapshin et al. reported the reaction of boron nitride with molten NaOH (melting point: 323 °C) under formation of sodium orthoborate and ammonia [19]. In the samples cured at 150 °C the coating was mostly intact, whereas the coating was decomposed after undergoing pyrolysis at 1450 °C.

The carbon sample derived from the R2 was investigated regarding porosity by means of the Archimedes water infiltration method, Hg-porosimetry and He-pycnometry. The results are summarized in Table 1. The Archimedes water infiltration method determined the open porosity to be 8.5% and a low density of 0.95 g/cm^3 for the bulk carbon material. This is consistent with the observation of floating in water (Fig. 11a, inset). In contrast, the results from the Hg-porosimetry measurement show a higher density of 1.22 g/cm^3 and a higher open porosity of 9.4% of the bulk carbon sample. This can be explained by the fact that meso- (diameter 2–50 nm) and macro-pores (diameter >50 nm) [20] are accessible for mercury. The water infiltration method on the other side only allows macro-pores larger than 100 nm to be accessible [20]. The result indicates the presence of pores, which are not accessible by the water infiltration method. The measurement of the bulk-carbon with He-pycnometry leads to a similar density of 1.19 g/cm^3. In order to determine the true density of the skeletal carbon the sample was pulverized in a ball mill, opening up all pores. After that procedure, the He-pycnometry and Hg-porosimetry show a density of 1.54 and 1.47 g/cm^3, respectively. This is a proof for the existence of a closed porosity, which is not accessible in the bulk form. A closed porosity of 22.7% (He-pycnometry) and 17.0% (Hg-porosimetry) in R2-carbon was calculated from the resulting densities from the bulk and powder according to Eq. (1):

$$\varepsilon' = 1 - \frac{\rho}{\rho_0} \tag{1}$$

ε' porosity; ρ density in bulk; ρ_0 density in powder.

The determination of the open porosity of the SiC/C composite by water infiltration and Hg-porosimetry yielded values of 13.7% and 16.2%, respectively (Table 1). The infiltrated preform had a fiber volume content of 47%. Due to the embedded dense SiC fibers, the open porosity of the carbon matrix is much higher than the one measured. In contrast, pure R2-carbon is characterized by an open porosity of only 8.5% and 9.4% (Table 1). This means the SiC fiber network increases the pore formation.

For an investigation of the carbon structure, Raman spectroscopy was locally measured at the edges of the pores and areas of

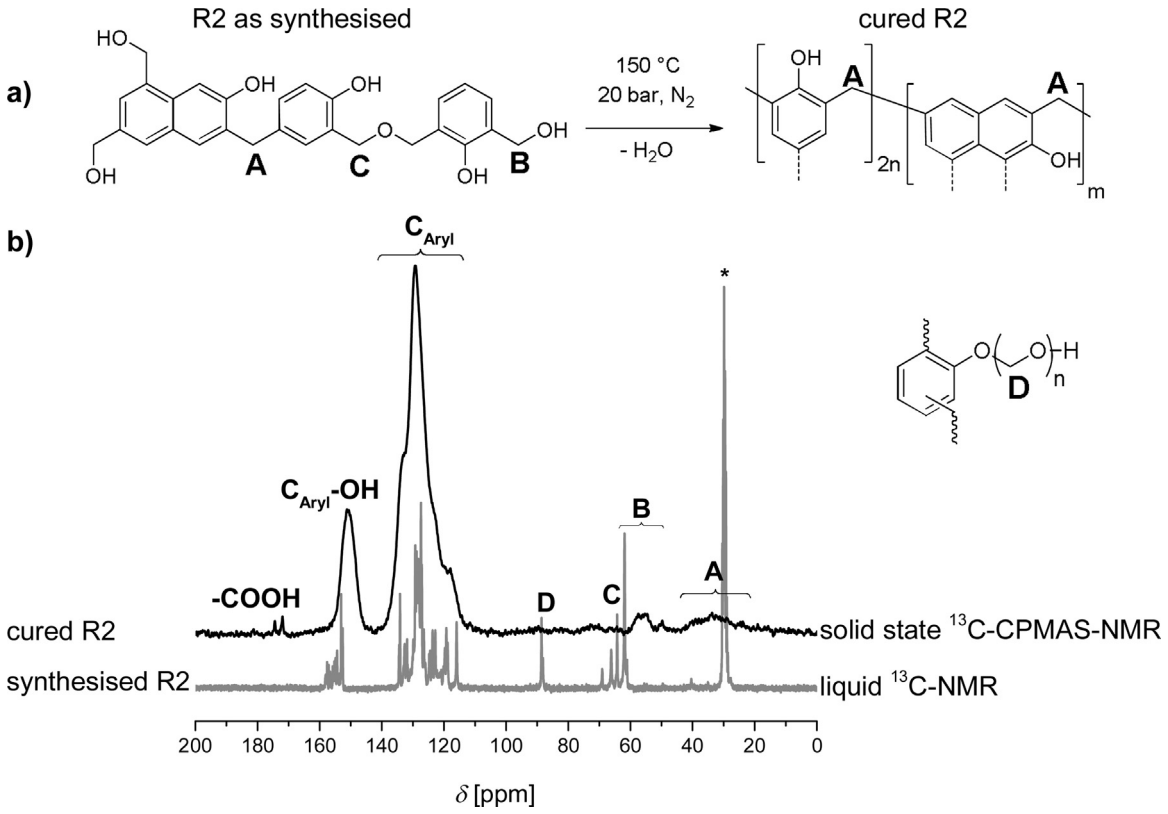

Fig. 9. Analysis of the chemical structure of R2: (a) possible structure of R2 as synthesized and cured, the dashed lines mark other possible positions for cross-linking; (b) liquid-^{13}C NMR spectra of R2 (grey) measured in aceton-d_6 (*) compared with the ^{13}C CPMAS spectra of R2 (black) cured at 150 °C with the assignment of the peaks to different carbon atoms in the polymer.

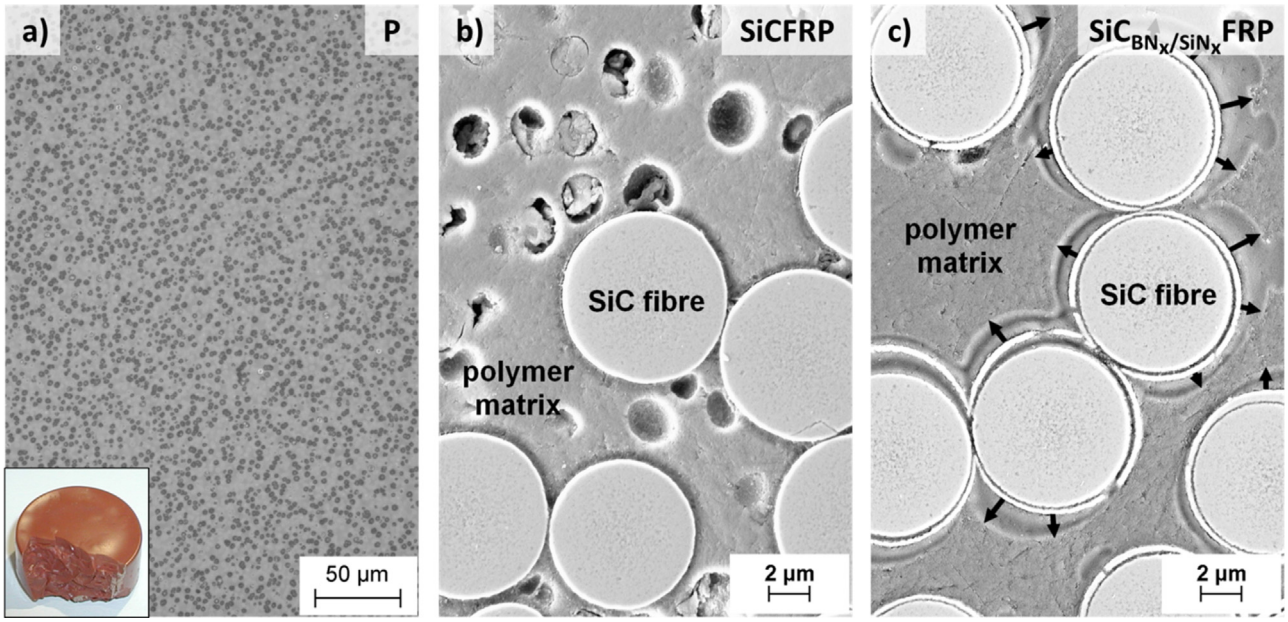

Fig. 10. Microstructure analysis of the pure polymer (P) and the polymer-matrix obtained of R2: (a) the picture of R2 after curing at 150 °C (20 bar N_2) (inset) and the optical microscopy image of the polymer (P); (b) the SEM image of the SiCFRP; (c) the SEM image of the $SiC_{BNx/SiNx}$FRP. The arrows show the shrinkage of the matrix.

compact carbon. Two typical bands can be seen in the Raman spectra. The D band around 1355 cm^{-1} can be attributed to terminal carbon (sp^3 hybridised C) of a graphene layer and carbon defects. Whereas the G band belongs to perfectly condensed aromatic rings of carbon (sp^2 hybridised C) [21]. A G band with a high intensity is characteristic for carbon with a high degree of graphitisation, which results in a low intensity-ratio between the maximum intensities I(D)/I(G). In pure carbon material a I(D)/I(G)-ratio of 1.32 was found compared with only 1.08 in a SiC/C matrix. This implies that the fiber network increases the degree of graphitisation in the carbon matrix. Additionally, at the edges of pores in both, the C and SiC/C matrix, a significant lower I(D)/I(G)-ratio of 0.87 and strongly

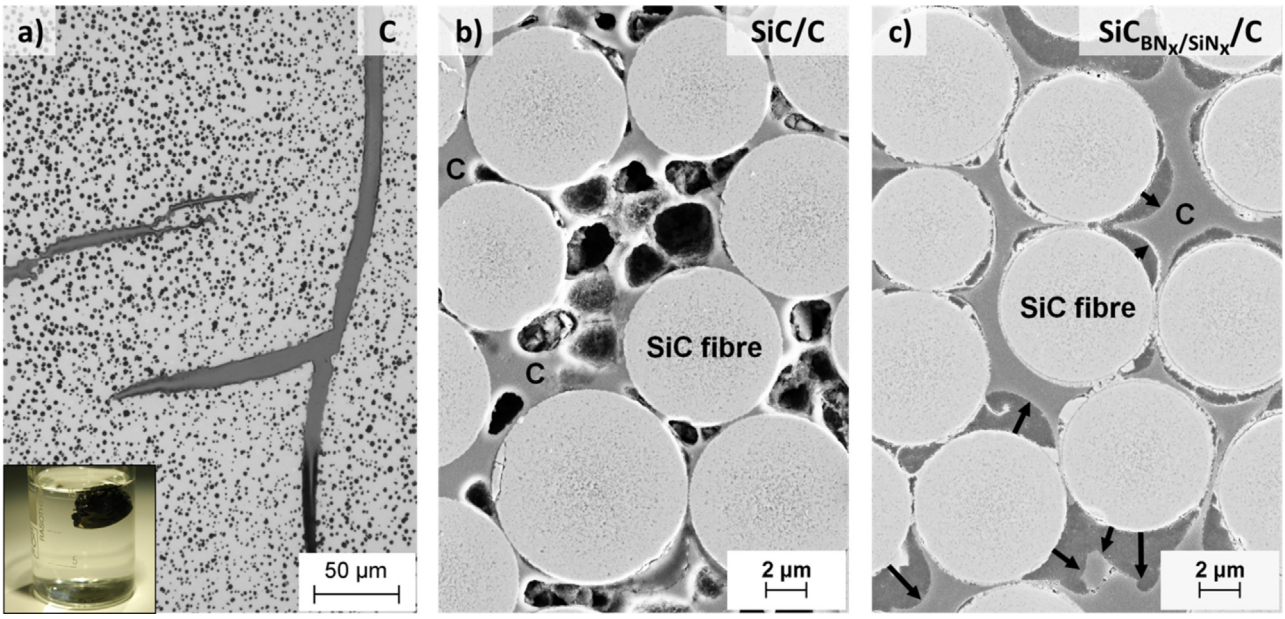

Fig. 11. Microstructure analysis of the pure carbon (C) and the carbon-matrix obtained from the R2: (a) picture of the carbon obtained from the R2, which is floating in water (inset) and the optical microscopy image of the carbon (C); (b) SEM image of the SiC/C composite; (c) SEM image of the $SiC_{BNx/SiNx}$/C composite, all pyrolysed at 1450 °C. The arrows show the shrinkage of the matrix.

Table 1
The densities and porosities of R2-carbon and SiC/C material.

	Density [g/cm^3]		Open porosity [%]	Closed porosity [%]	Density [g/cm^3]	Open porosity [%]
Material	C bulk	C powder	C bulk	C	SiC/C bulk	SiC/C bulk
Water infiltration	0.95	*	8.5	*	1.99	13.7
Hg-porosimetry	1.22	1.47	9.4	17.0	1.93	16.2
He-pycnometry	1.19	1.54	*	22.7	2.40	*

*Cannot be determined by means of this method.

increased base line was determined. This was not found in resol formulations void of any β-naphthol [3]. These findings suggest that the addition of β-naphthol during the resol synthesis seems to have an effect on the degree of graphitisation of the carbon matrix after pyrolysis. The higher peak of the G band and the raised base line can also be found for the pyrolysed naphthalene-derived mesophase pitch in contrast to pitch that obtained from alkybenzene containing coal tar [22].

3.4. Analysis of the liquid silicon infiltration of pure carbon and of the carbon matrix (Step III)

The pyrolysis of the pure R2 sample generated a glassy type carbon with a higher degree of graphitisation at the edges of the pores, a high closed porosity and an open porosity of only 9.4% (He-pycnometry Table 1). In order to obtain a better understanding for the liquid silicon infiltration of closed porous carbon foams, the pure R2-carbon sample was siliconised under an excess of liquid silicon under the same processing conditions as the SiC/C composite was (Fig. 12a, inset). Long cavities of the micrometer scale, which penetrate the pyrolysed carbon of the R2 were filled with a liquid silicon and reached the inside of the closed porous carbon foam (Fig. 12a). A 3–20 µm thick inhomogeneous SiC layer developed on the interface, which was visible with partly rounded shapes on the carbon side due to the infiltrated pores. In some areas pores were interconnected, resulting in a deep conversion of the carbon matrix to create elongated SiC domains with lengths of up to 20 µm. There was no complete conversion of the carbon with liquid silicon. By comparison, the SiC formation from graphite with liquid silicon shows similar processes taking place, which leads to a similar morphology of the SiC. Glassy carbon leads to a 10 µm thick SiC layer, whereas polycrystalline graphite resulted in a SiC layer-thickness of 15 µm when reacted with liquid silicon at 1600 °C (Ar). It has been shown, that the formation of the SiC layer from graphite is influenced by the infiltration of pores [23].

Liquid silicon was successfully infiltrated in the SiC/C composite with uncoated fibers. This is a result of the good wetting capabilities of liquid silicon on carbon and silicon carbide surfaces. The contact angles were measured to be 31° on glassy carbon and 37° on silicon carbide. This allows silicon to be infiltrated in the SiC/C composite by capillary forces. The content of residual silicon within the matrix was only 15.8 vol.-%. Compared to the silicon infiltration experiments on pure specimens of the R2 carbon, the fiber reinforcement leads to a sufficiently high open porosity over the entire composite. This high porosity and a dissolution of the partly closed porous carbon led to homogenous infiltration and complete conversion of the carbon matrix to silicon carbide (Fig. 12b). The unprotected SiC fibers were partly attacked by silicon. These attacks started along the boundaries of grains by the solution of small silicon carbide crystals and precipitation at lager silicon carbide crystals within the matrix. The silicon did not infiltrate the matrix with coated fibers (Fig. 12c). During the analysis it was concluded, that this behavior has a strong correlation to the degradation of the coating during pyrolysis. As a result of the degradation, the boron nitride layer was partly exposed to liquid silicon which was repelled due to a high contact angle of 135° on boron nitride.

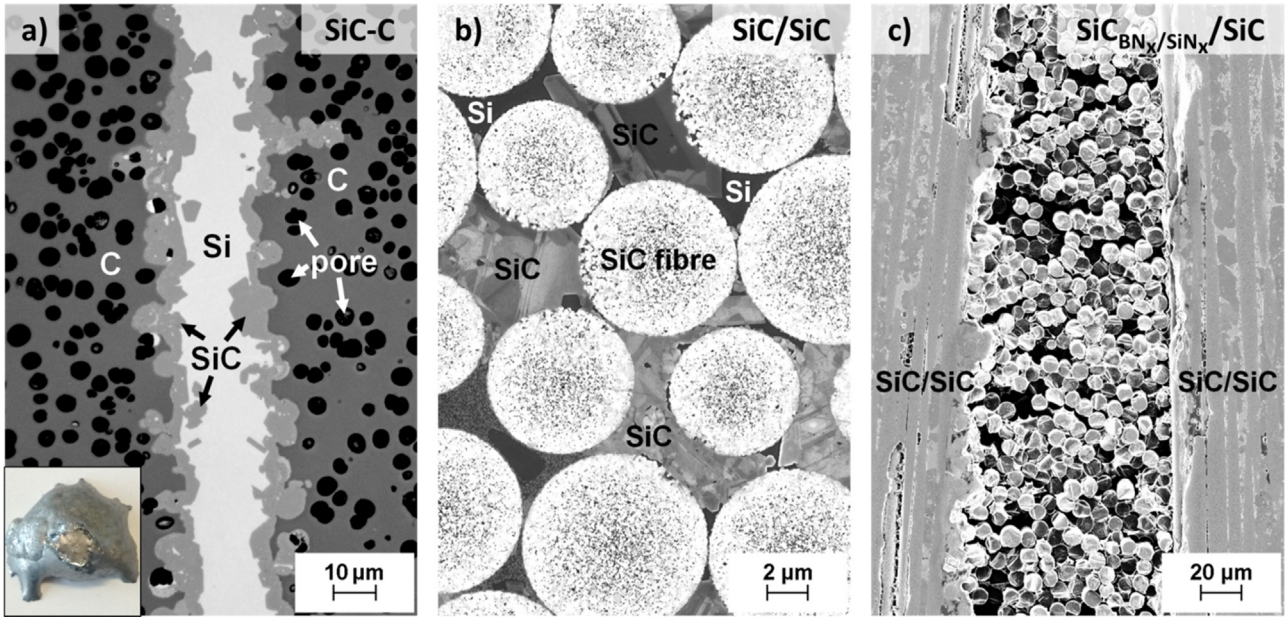

Fig. 12. Microstructure analysis of liquid silicon infiltration of R2-carbon and R2-carbon-matrix: (a) picture of the siliconised R2-carbon (inset) and the optical microscopy image of the interface between the silicon and SiC; (b) SEM image of the SiC/SiC composite; (c) SEM image of the SiC/SiC composite with a BN_x/SiN_x fiber-coating. The section with coated fibers was not infiltrated and remained in the pyrolysed stage.

4. Conclusion

A SiC/SiC composite was manufactured with a novel BN_x/SiN_x fiber coating and a tailored phenolic resin (R2). The base materials as well as the three stages of the composite during the LSI process were investigated.

The fiber coating was applied by means of low-pressure chemical vapor deposition by utilizing gaseous chlorine free precursors. After the deposition the double coating is amorphous. The coating was exposed to a heat treatment in order to examine the stability. Only the SiN_x coating crystallized to α-Si_3N_4, whereas the BN_x coating remains amorphous.

After undergoing pyrolysis, the R2 polymer developed a closed porosity of 22.7% and an open porosity of only 9.4%. Within the uncoated SiC fibers the open porosity was increased to 16.2%. This was a result of a strong fiber/matrix bonding during curing and pyrolysis. In the pyrolysed stage the pores showed diameters between 1 and 4.5 µm. Although a large amount of pores still remained closed, they were accessible for the liquid silicon. The high mass yield of the polymer promoted a SiC matrix with low amounts of residual silicon.

For composites with BN_x/SiN_x-coated fibers the coating/matrix bonding was considerably lower, which leads to the interface debonding. The shrinkage of the volume during the curing process was unhindered and the formation of new pores was locally supressed. Hollow channels along the coated fiber surface were formed. During the pyrolysis a continued degradation of the coating took place as a result of the reaction between the BN_x coating and the NaOH of the phenolic resin. The exposed coatings were unsuitable for the subsequent infiltration of liquid silicon. Due to the high contact angle between the silicon and boron nitride, the silicon did not infiltrate the section of the coated fibers.

For further investigations a NaOH-free resin is required to prevent a decomposition of the boron nitride fiber coating. In addition, $SiC_{BNx/SiNx}$ fiber composites require a carbon precursor with a higher adhesion to the SiN_x coating and a reduced shrinkage of the volume with an increased foaming tendency during the curing process. Furthermore, a gradient of the fiber coating in the B-N-Si system should be developed, which would moderate the residual stresses and improve the cohesive bonding within the coating.

Acknowledgements

The financial support for the SiCaFis project (FR 1355/7-1, NE 1663/3-1 and SP 392/38-1) by the Deutsche Forschungsgemeinschaft (DFG) is gratefully acknowledged. We also want to thank Dr. Enrico Dietzsch for performing the Hg-porosimetry measurements and Prof. Dr. Klaus Stöwe for giving us the opportunity to measure the density with He-pycnometry. An additional acknowledgement goes to Anne Schulze for preparing the thin sections for TEM investigations analysis.

References

[1] R. Kochendörfer, Liquid silicon infiltration-a aast and low cost CMC manufacturing process, in: Proc. 8th Int. Conf. on Composite Materials (ICCM 8), Honolulu/Hawaii, July 15–19, 1991.
[2] W. Krenkel, F.H. Gern, Microstructure and Characteristics of CMC Manufactured via the Liquid Phase Route, in: Proceedings of the Ninth International Conference on Composite Materials, Madrid, Spain, July 12–16, 1993, vol. II: Ceramic Matrix Composites and Other Systems, 2015, pp. 173–181.
[3] L. Wöckel, T. Ebert, B. Mainzer, M. Frieß, D. Koch, K. Roder, D. Wett, D. Nestler, G. Wagner, S. Spange, Investigation of different phenolic resins and their behavior during pyrolysis to form SiC/C-composites, Mater. Sci. Forum 825–826 (2015) 240–248.
[4] K. Roder, D. Nestler, D. Wett, B. Mainzer, M. Frieß, L. Wöckel, T. Ebert, G. Wagner, D. Koch, S. Spange, Development of a SiN_x-based barrier coating for SiC fibres, Mater. Sci. Forum 825–826 (2015) 256–263.
[5] B. Mainzer, M. Frieß, K. Roder, D. Wett, D. Nestler, G. Wagner, L. Wöckel, T. Ebert, S. Spange, D. Koch, Development and characterization of phenolic resin based liquid silicon infiltrated SiC/SiC composites with SiNx fibre coating, Mater. Sci. Forum 825–826 (2015) 224–231.
[6] M.T. Duffy, S. Berkman, G.W. Cullen, R.V. D'Aiello, H.I. Moss, Development and evaluation of refractory CVD coatings as contact materials for molten silicon, J. Cryst. Growth 50 (1980) 347–365.
[7] T.M. Besmann, S. Shanmugham, E.R. Kupp, D.P. Stinton, Approach to inherently stable interfaces for ceramic matrix composites, in: W.S. Johnson (Ed.), Proc. 11th Technical Conference on Composite Materials, Technomic Pub., Lancaster, PA, 1996, pp. 371–380.
[8] UBE INDUSTRIES, LTD, Tyranno Fiber®, product brochure.
[9] E. Buet, C. Sauder, S. Poissonnet, P. Brender, R. Gadiou, C. Vix-Guterl, Influence of chemical and physical properties of the last generation of silicon carbide

fibres on the mechanical behaviour of SiC/SiC composite, J. Eur. Ceram. Soc. 32 (2012) 547–557.
[10] S. Nakashima, H. Harima, Raman investigation of SiC polytypes, Phys. Status Solidi A 162 (1997) S39–S64.
[11] B.S. Mitchell, An Introduction to Materials Engineering and Science for Chemical and Materials Engineers, Wiley, Hoboken, 2004, ISBN 0-471-43623-2.
[12] M.-F. Grenier-Loustalot, S. Larroque, P. Grenier, D. Bedel, Phenolic resins: 4. Self-condensation of methylolphenols in formaldehyde-free media, Polymer 37 (1996) 955–964.
[13] M.-F. Grenier-Loustalot, S. Larroque, P. Grenier, Phenolic resins: 5. Solid-state physicochemical study of resoles with variable FP ratios, Polymer 37 (1996) 639–650.
[14] R. Rego, P.J. Adriaensens, R.A. Carleer, J.M. Gelan, Fully quantitative carbon-13 NMR characterization of resol phenol-formaldehyde prepolymer resins, Polymer 45 (2004) 33–38.
[15] X. Zhang, A.C. Potter, D.H. Solomon, The chemistry of novolac resins-V. Reactions of benzoxazine intermediates, Polymer 39 (1998) 399–404.
[16] I.S. Chuang, G.E. Maciel, Carbon-13 NMR investigation of the stability of a resol-type phenol-formaldehyde resin toward formalin, toward base, and toward nonoxidizing or oxidizing acid, Macromolecules 24 (1991) 1025–1032.
[17] J.C. Margiotta, D. Zhang, D.C. Nagle, C.E. Feeser, Formation of dense silicon carbide by liquid silicon infiltration of carbon with engineered structure, J. Mater. Res. 23 (2008) 1237–1248.
[18] K.M. Taylor, Hot pressed boron nitride, Ind. Eng. Chem. 47 (1955) 2506–2509.
[19] A.V. Lapshin, A.M. Germanskii, S.P. Bogdanov, Interaction of boron nitride with molten sodium hydroxide, Glass Phys. Chem. 30 (2004) 202–206.
[20] J. Rouquerol, D. Avnir, C.W. Fairbridge, D.H. Everett, J.M. Haynes, N. Pernicone, J.D.F. Ramsay, K.S.W. Sing, K.K. Unger, Recommendations for the characterization of porous solids (technical report), Pure Appl. Chem. 66 (1994) 1739–1758.
[21] A.C. Ferrari, J. Robertson, Interpretation of Raman spectra of disordered and amorphous carbon, Phys. Rev. B 61 (2000) 14095–14107.
[22] M. Dumont, G. Chollon, M.A. Dourges, R. Pailler, X. Bourrat, R. Naslain, L. Bruneel, M. Couzi, Chemical, microstructural and thermal analyses of a naphthalene-derived mesophase pitch, Carbon 40 (2002) 1475–1486.
[23] A. Favre, H. Fuzellier, J. Suptil, An original way to investigate the siliconizing of carbon materials, Ceram. Int. 29 (2003) 235–243.